

2009

# Quantitative prediction of body surface potentials from myocardial action potentials using a summed dipole model

Charles F. Babbs

*Purdue University*, [babbs@purdue.edu](mailto:babbs@purdue.edu)

Follow this and additional works at: <http://docs.lib.purdue.edu/bmepubs>



Part of the [Biomedical Engineering and Bioengineering Commons](#)

---

## Recommended Citation

Babbs, Charles F, "Quantitative prediction of body surface potentials from myocardial action potentials using a summed dipole model" (2009). *Weldon School of Biomedical Engineering Faculty Publications*. Paper 62.  
<http://docs.lib.purdue.edu/bmepubs/62>

This document has been made available through Purdue e-Pubs, a service of the Purdue University Libraries. Please contact [epubs@purdue.edu](mailto:epubs@purdue.edu) for additional information.

# Quantitative prediction of body surface potentials from myocardial action potentials using a summed dipole model

**Charles F. Babbs, MD, PhD**

*Department of Basic Medical Sciences and Weldon School of Biomedical Engineering,  
Purdue University, West Lafayette Indiana*

Cardiovascular Engineering 9, 59-71, 2009

## **Abstract**

This paper demonstrates quantitatively, using streamlined mathematics, how the transmembrane ionic currents in individual cardiac muscle cells act to produce the body surface potentials of the electrocardiogram (ECG). From fundamental principles of electrostatics, anatomy, and physiology, one can characterize the strength of apparent dipoles along a wavefront of depolarization in a local volume of myocardium. Net transmembrane flow of ionic current in actively depolarizing or repolarizing tissue induces extracellular current flow, which sets up a field of electrical potential that resembles that of a dipole. The local dipole strength depends upon the tissue cross section, the tissue resistivity, the resting membrane potential, the membrane capacitance, the volume fraction of intracellular fluid, the time rate of change of the action potential, and the cell radius. There are no unknown, "free" parameters. There are no arbitrary scale factors. Body surface potentials are a function of the summed local dipole strengths, directions, and distances from the measuring point. Calculations of body surface potentials can be made for the scenarios of depolarization (QRS complex), repolarization (T wave) and localized acute injury (ST segment shifts) and agree well with experimentally measured potentials. This simplified predictive dipole theory provides a solution to the forward problem of electrocardiography that explains from a physiological perspective how the collective depolarization and repolarization of individual cardiac muscle cells create body surface potentials in health and disease.

**Key words** Action potential; Body surface potential mapping; Electrocardiography; Forward problem; Ionic currents; Transmembrane potential; Vector

## Introduction

The present paper is written for students of engineering, physiology, and medicine at all levels who have had difficulty visualizing the exact connection for between the excursion of transmembrane potentials in cardiac muscle from about zero to about  $-100$  millivolts to the waveform of electrocardiogram with a maximal R-wave amplitude of about 2 millivolts at the body surface. Creation of a compact, quantitative model for the genesis of the electrocardiogram (ECG) that is intuitively related to anatomy and physiology has been an open problem<sup>1</sup>. Still lacking is a mathematically accessible explanation of the causal link between the transmembrane current in individual cardiomyocytes and the body surface ECG.

This so-called "forward problem of electrocardiography" has attracted a broad community of thinkers over the last quarter century, who have considered the genesis of the electrocardiogram from the perspective of physics and engineering. The extensive development of numerical methods and computer hardware has made the study of very complex models possible, including detailed models of cardiac muscle cells and ion channels, cardiac and non-cardiac tissues (biodomains), and the three dimensional gross anatomy of the thorax<sup>2</sup>. Notable examples of complex solutions to the forward problem include those of Plonsey<sup>3</sup>, Geselowitz<sup>4</sup>, Rudy<sup>5</sup>, Gulrajani<sup>6</sup>, Selvester<sup>7</sup>, Barr<sup>8</sup>, Gelernter and Swihart<sup>9</sup> (1964), and Miller and Geselowitz<sup>10</sup>. While technically successful, these mathematical models are exceedingly complex and far beyond the understanding of most students of physiology and medicine.

Most closely matching the objectives of the present paper was the work of Miller and Geselowitz<sup>10</sup> in 1978. They assumed that a net current flows in an intracellular network from regions of higher intracellular potentials to regions of lower intracellular potentials. The spatial distribution of intracellular potentials was calculated, and the boundary value problem was then solved to obtain transmembrane currents. The ventricles of the heart were represented in detail by a three-dimensional array of approximately 4000 points. (However, for simplicity, the heart model was divided into 23 regions, each of which was represented by a single dipole located at the centroid of the region.) In the calculations of Miller and Geselowitz simulation potentials were calculated in arbitrary units, and a scale factor was determined to give a maximum potential of approximately 2 millivolts. In this sense the theoretical predictions of body surface potentials were not expressed in absolute but in relative units. This important work did, however, succeed in demonstrating that body surface potentials begin at the level of the cellular action potential, as is intuitively obvious.

Such approaches to solving the forward problem include dozens to hundreds of equations and thousands to hundreds of thousands of finite elements of tissue in three-dimensional space<sup>2</sup>. These models have become exercises in sophisticated computer science far beyond the usual domains of physiology and medicine. They have also tended to express results for computed body surface potentials in arbitrary units<sup>8,9</sup>, blurring the question of exactly how many millivolts of electrical potential difference are expected between

arbitrary points A and B on the chest wall, given known normal or abnormal cardiac electrophysiology.

The present research re-explores the same intellectual territory from a physiological perspective in a much fewer number of steps, using substantially streamlined mathematics. It nevertheless leads to explicit, quantitative predictions of body surface potentials in millivolts, and connects the strength of the surface signal in millivolts to the strength of the transmembrane action potential in millivolts and commonly known physiologic parameters such as specific membrane capacitance per square centimeter. The objective is capture the essence of the physical link between the transmembrane action potentials of cardiac myocytes and the body surface potentials of the electrocardiogram in a rigorous and predictive way.

## Theory

### The effective local dipole for a strip of cardiac muscle

Consider first a one-dimensional column of cardiac muscle undergoing electrical excitation or recovery\*. Fig. 1 shows a thin column of ventricular muscle cells extending an equal distance,  $a$ , on either side of a boundary between two zones of tissue in different electrophysiological states. For example, muscle in zone 1 may be actively depolarizing, while muscle in zone 2 is in a resting state. The cross sectional area of the column,  $A$ , is small enough with respect to its length,  $2a$ , that the border between zones 1 and 2 can be regarded as a flat plane. At any particular instant in time the transmembrane action potentials and in turn the slopes of the transmembrane action potentials in the two zones may differ. Consider the net outward transmembrane current,  $i$ , in each zone flowing from the intracellular to extracellular spaces. During repolarization or recovery (the T wave of the electrocardiogram) this current is positive, indicating a net outflow of positive ions across cell membranes. During depolarization or excitation (the QRS complex of the electrocardiogram) this current is negative, indicating a net inflow of positive ions, in particular sodium ions, across cell membranes.

---

\* Because the overwhelming majority of cardiac mass is composed of working cardiac muscle cells, rather than SA or AV nodal cells or Purkinje fibers, the voltage and current waveforms of such working cardiomyocytes are most relevant to the present problem. His bundle potentials, for example, cannot be observed on the body surface ECG and require intracardiac recording.

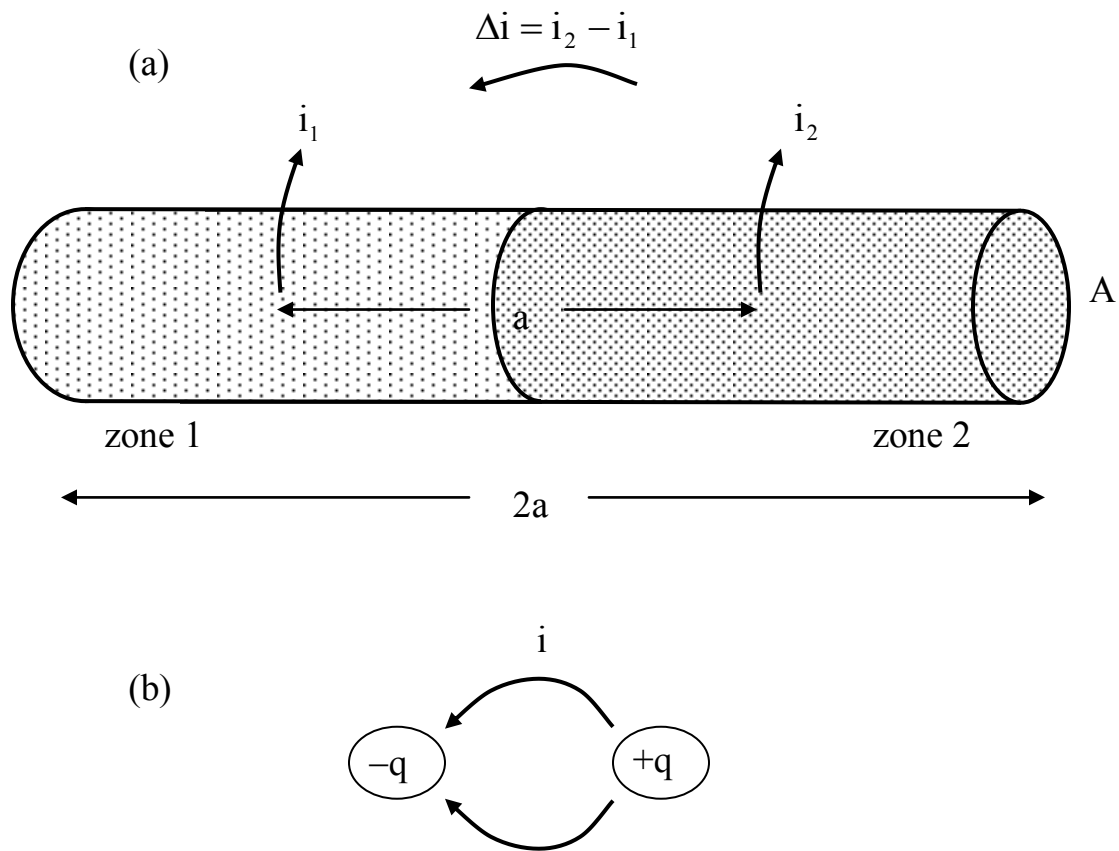


**Fig. 1.** (a) Thin cylinder of cardiac muscle divided into two zones, 1 and 2, having different cellular transmembrane potentials and different instantaneous transmembrane currents,  $i_1$  and  $i_2$ . If transmembrane current flow in the two zones is not equal, the difference in current will flow axially in the extracellular space, creating an effective dipole between the zones. Outflow from one zone equals inflow to the other. (b) The pattern of current flow resembles that created by a dipole having charge separation distance,  $a$ , equal to the distance between the center of zone 1 and the center of zone 2.

As indicated in Fig. 1(a), if  $i_1$  is not equal to  $i_2$  then the difference  $\Delta i = i_2 - i_1$  will flow axially from membrane capacitance on the right to membrane capacitance on the left, as if created by a dipole having a cluster of positive charges concentrated at one point to the right of the border and a cluster of negative charges concentrated at a mirror image point to the left of the border (Fig. 1(b)). Our strategy is to find the axial current  $\Delta i = i_2 - i_1$  in terms of physiologic variables and then find the equivalent dipole, composed of simple point charges,  $+q$  and  $-q$ , separated by distance,  $a$ , which would produce this same axial current flow. The electric potential at any distance and any angle from such a dipole is well known, and easy to calculate. If we can find the equivalent dipole for the muscle column, then we can find the contribution of the muscle column to body surface

potentials and the electrocardiogram. Summing the potentials contributed by multiple muscle columns throughout the heart solves the forward problem.

Consider either zone of Fig. 1(a), having volume equal to the product of area times length,  $Aa$ , where zones 1 and 2 in the model of Fig. 1 are defined as having equal lengths,  $a$ . Each zone has characteristic transmembrane potential,  $V$ , total membrane charge,  $Q$ , and total membrane capacitance,  $C$ . By the fundamental definition of capacitance we have  $Q = CV$ . By definition the transmembrane current,  $i$ , is the time rate of change in membrane charge  $Q$ . Hence the instantaneous transmembrane current in either zone is

$$i = \frac{dQ}{dt} = -C \frac{dV}{dt} \quad \text{or} \quad (1)$$

$$i = -C\dot{V}.$$

The negative sign in (1) indicates that when transmembrane potential is decreasing the cell is becoming more polarized (outside positive, inside negative), which means that there is positive outward transmembrane current,  $i$ . Since  $C$  is a constant, transmembrane current is the product of membrane capacitance and the slope  $dV/dt$  of the transmembrane potential. This slope in units of Volts/sec is often abbreviated " $\dot{V}$ ", the "dot" symbol over the letter  $V$  indicating the first time derivative. (Definitions of these and other variables are summarized in Appendix 3: nomenclature.)

The total membrane capacitance  $C$  in either zone is the product of the well known specific capacitance,  $C_m$ , of biological membranes per unit area (about  $1 \mu\text{F}/\text{cm}^2$ )<sup>11</sup> and the total surface area of muscle cells in the half column volume  $Aa$ . Using a cylindrical model for cardiac muscle cells of radius,  $r_c$ , comprising volume fraction of muscle tissue,  $\sigma_{icf}$ , of muscle tissue, the total area of cell surface membrane per unit volume of tissue (from Appendix 1) is simply

$$\text{area/volume} = \frac{2\sigma_{icf}}{r_c}. \quad (2)$$

The total cell membrane area in volume  $aA$  of the thin cylinder model is therefore

$$A_c = \frac{2aA\sigma_{icf}}{r_c}. \quad (3)$$

Using  $C = C_m A_c$  in (1) we can solve for the current flowing out of cells in either zone as,

$$i = -C\dot{V} = -\frac{2aAC_m\sigma_{icf}}{r_c} \cdot \dot{V}, \quad (4)$$

in terms of very well characterized anatomic and physiologic variables, including most importantly, the slope of the transmembrane action potential,  $\dot{V} = dV/dt$ .

Now the axial current flowing between the two zones is the difference in transmembrane currents

$$\Delta i = i_2 - i_1 = \frac{2aAC_m\sigma_{icf}}{r_c} \cdot (\dot{V}_1 - \dot{V}_2). \quad (5)$$

The next step is to find the local dipole within the extracellular milieu that would create the same axial current flow. Electrical fields surrounding a classical dipole, in which point charges  $-q$  and  $+q$  are separated in space by distance  $a$ , are easily calculated<sup>12</sup>. The product,  $p = aq$  is known as the dipole moment. The electrical potential in the neighborhood of such a dipole at an arbitrary point, P, located distance,  $r$ , from the midpoint of the dipole and making angle,  $\theta$ , with respect to the dipole axis, is

$$V_p = kq \left\{ \frac{1}{\sqrt{r^2 + a^2/4 - ra \cdot \cos(\theta)}} - \frac{1}{\sqrt{r^2 + a^2/4 + ra \cdot \cos(\theta)}} \right\}. \quad (6a)$$

This exact expression is derived in Appendix 2. Here  $k$  is a constant of nature that depends upon the electrical permittivity of free space and the dielectric constant of the surrounding medium<sup>12</sup>. For far field points P where  $r \gg a$ , (6a) simplifies to the usual textbook formula,

$$V_p \cong \frac{kp}{r^2} \cos(\theta), \quad (6b)$$

where  $k$  is the permittivity constant and  $p$  is the dipole moment.

We can now find the equivalent dipole with charge separation,  $a$ , for which the total current flowing past the mid-plane of the dipole is the same as the current flowing from zone 1 into zone 2 in expression (5). At the mid-plane of a dipole all current flow is parallel to the axis of the column, allowing for easier integration of the current. Such a dipole would set up an electric field that can be specified exactly by (6). In turn, the potentials created by similar columns throughout the heart can be found and summed to generate a body surface potential map for the heart as a whole.

To find the equivalent dipole, imagine a circular ring of the dipole's mid-plane at distance  $r$  from the center point and having circumference  $2\pi r$ , thickness  $r d\theta$ , and height  $dr$ , as shown in Fig. 2. The extracellular current flowing through the ring equals the voltage difference across the ring in the " $r\theta$  direction", parallel to the axis of the column, divided by the resistance of the ring. Both of these components can be specified. The voltage

difference across the ring is  $-\frac{\partial}{\partial\theta}(V_p(r, \theta))d\theta$ , where the angle,  $\theta$ , of the mid-plane is 90 degrees. As shown in Appendix 2 the partial derivative of the dipole potential field (6a) at the midline ( $\theta = 90^\circ$ ) is

$$-\frac{\partial}{\partial\theta}V_p(r, 90^\circ) = \frac{kpr}{(r^2 + a^2/4)^{3/2}}. \quad (7)$$

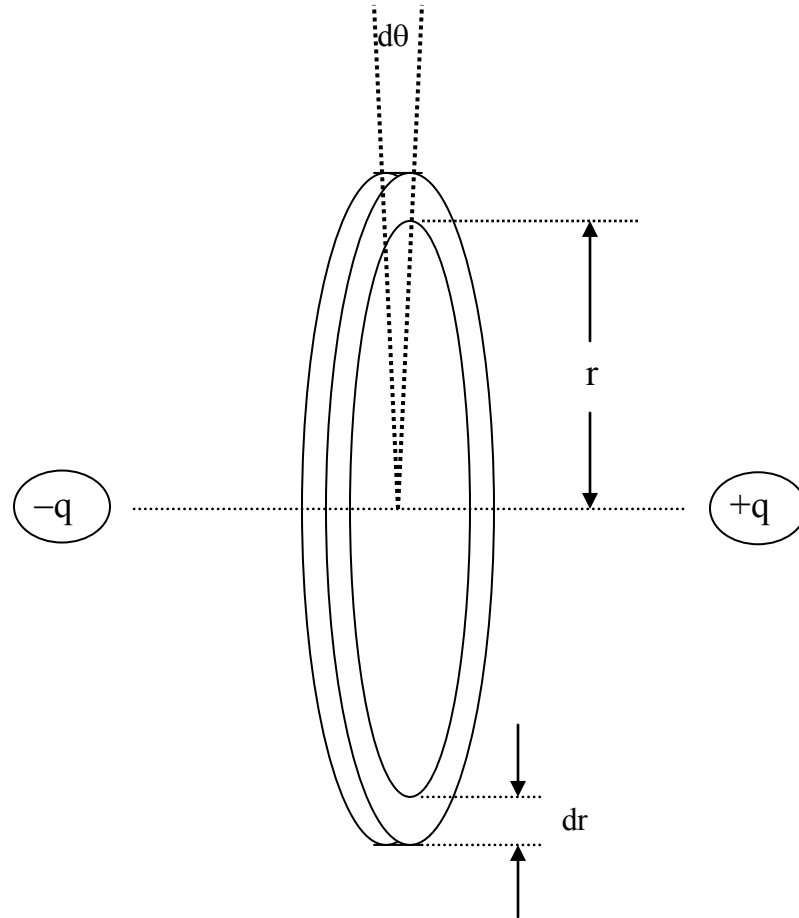


**Fig. 2.** Ring-shaped slice of space for calculating differential current increment,  $di$ , at radial distance,  $r$ , flowing from positive to negative poles of dipole  $(-q) - (+q)$ . The total current is  $\int_{r=0}^{\infty} di$ , as shown in Equations (7) through (9).

The resistance of the ring perpendicular to the mid-plane equals the local tissue resistivity,  $\rho$ , multiplied by the width of the ring (in the direction of current flow) and divided by the ring cross section<sup>1</sup>, or

$$R_{\text{ring}} = \rho \frac{rd\theta}{2\pi r dr}. \quad (8)$$

Hence the current passing through the differential ring at radius  $r$  along the mid-plane is the voltage difference across the ring, divided by its resistance, or

$$di = \frac{\frac{kpr}{(r^2 + a^2/4)^{3/2}} \cdot d\theta}{\frac{\rho r d\theta}{2\pi r dr}} = \frac{2\pi kpr}{\rho(r^2 + a^2/4)^{3/2}} dr. \quad (9a)$$

The total axial current flowing from the source into the sink at all radii is the integral of (9a)<sup>13</sup>

$$i = \int_0^\infty di = \frac{2\pi kp}{\rho} \int_0^\infty \frac{r}{(r^2 + a^2/4)^{3/2}} dr = \frac{4\pi kp}{\rho a}. \quad (9b)$$

However, we also know from expression (5) that the total axial current is

$$\frac{2aAc\sigma_{\text{icf}}}{r_c} (\dot{V}_1 - \dot{V}_2),$$

so equating (5) and (9b) we can deduce the dipole moment product,  $kp$ , for the muscle column as

$$kp = \frac{1}{2\pi} \cdot \frac{\rho a^2 AC_m \sigma_{\text{icf}}}{r_c} (\dot{V}_1 - \dot{V}_2). \quad (10)$$

The parameters governing the dipole moment product,  $kp$ , in expression (10) are all related to known anatomy and physiology. They include the cross sectional area and distance, the tissue resistivity,  $\rho$ , the slopes,  $\dot{V}$ , of transmembrane potentials during various normal or pathological states, the specific membrane capacitance per unit area,  $C_m$ , the volume fraction of the intracellular space,  $\sigma_{\text{icf}}$ , and the radius of a typical cylindrical cardiac muscle cell,  $r_c$ . By using the numerical value for  $kp$  from (10) in Equation (6) it is now possible to determine the remote potential generated by each such tissue volume within the heart. Fields of multiple muscle columns throughout the heart will sum to create an overall field of body surface potentials and the electrocardiogram.

In particular, if there are many such columns of tissue,  $n$ , within the heart at any instant of time, then combining expressions (6b) and (10), the local field at measuring point,  $P$ , is simply

$$V(P) = \frac{\rho C_m \sigma_{icf}}{2\pi r_c} \cdot \sum_n A_n a_n^2 (\dot{V}_1 - \dot{V}_2)_n \cdot \frac{\cos(\theta_n)}{r_n^2}. \quad (11)$$

Hence, one can use a computer program to divide a model of the heart of any size, shape, and pathology into an arbitrary number of segments, and predict quantitatively for any particular scenario the entire body surface potential map, using known textbook values for the parameters. In this sense expression (11) is an approximate quantitative solution to the forward problem of electrocardiography.

### Electrical excitation—the QRS complex

Consider in particular the events during ventricular excitation at the time of the QRS complex of the electrocardiogram. Fig. 3 shows a thin column of ventricular muscle cells stretching from the endocardium to the epicardium\*. The ventricular wall may be regarded as a honeycomb like array of such columns (Fig. 3, inset). Let  $V_m$  indicate the resting transmembrane potential, where  $V_m \approx -90$  millivolts. A wavefront of activation proceeds from left to right, with conduction velocity  $v$  ( $\sim 100$  cm/sec, indicated by the straight arrow). Cells in the column are in one of three states. Cells on the left are completely depolarized with transmembrane potential  $V \sim 0$  and  $\dot{V} = 0$ . Cells on the right are still in the resting state with transmembrane resting potential,  $V = V_m$  and  $\dot{V} = 0$ . Cells in the middle transition zone are actively depolarizing. They have an intermediate potential with  $\dot{V} > 0$ . This transition zone, or active band, moves from left to right with velocity,  $v$ . In it there is a strong current representing the discharge of membrane capacitance through fast sodium channels, as sodium ions enter depolarizing myocytes in the active band<sup>14</sup>.

The width,  $a$ , of the transition zone is equal to the product of the conduction velocity and the depolarization time  $t_{\text{depol}}$ , which equals the duration of Phase 0 of the cardiac action potential. This brief duration can be estimated by dividing  $-V_m$  by the rate of rise of the action potential during Phase 0. In physiology this slope,  $dV/dt$  in Phase 0, is abbreviated  $\dot{V}_{\text{max}}$ . Thus we can specify the depolarization time

$$t_{\text{depol}} = \frac{V_m}{\dot{V}_{\text{max}}} \quad (12)$$

---

\* Individual cells in the column are not necessarily aligned with the column axis, and indeed owing to the diagonal wrapping of cardiac muscle fibers around the ventricles, the cells are generally oriented perpendicular to the axes of such columns.

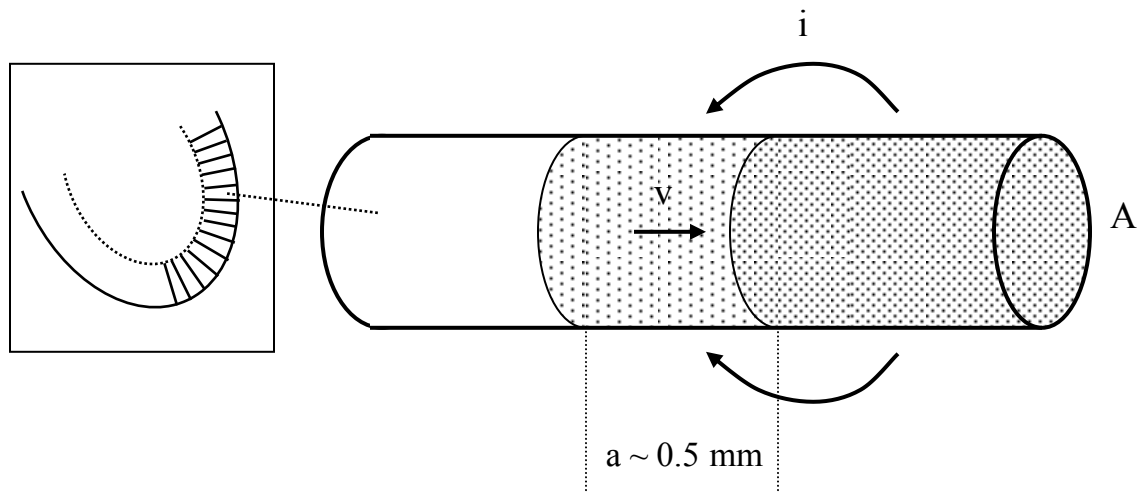


**Fig. 3.** A wavefront of depolarization proceeding from left to right in a column of cardiac muscle tissue, stretching from endocardium to epicardium of the left ventricular wall (inset), induces current,  $i$ , to flow into the interiors of actively depolarizing cells in an active band of width,  $a$ . Owing to the diagonal wrapping of cardiac muscle fibers around the ventricles, the cells are generally oriented perpendicular to the axes of such columns.

and the width of the transition zone

$$a = vt_{\text{depol}} = \frac{v \cdot V_m}{\dot{V}_{\text{max}}} \quad (13)$$

Approximate values for conduction velocity, resting membrane potential, and  $\dot{V}_{\text{max}}$  in mammalian hearts are 100 cm/sec, 0.1 volt, and 200 V/sec, respectively<sup>3-5</sup>. The active band just behind the leading edge of the depolarization wavefront has width

$$a = \frac{v \cdot V_m}{\dot{V}_{\text{max}}} \approx \frac{100 \frac{\text{cm}}{\text{sec}} \cdot 0.1 \text{ Volt}}{200 \frac{\text{Volt}}{\text{sec}}} = 0.05 \text{ cm}$$

or about half a millimeter, and passes through a fixed point in  $V_m / \dot{V}_{\text{max}} = 0.5$  milliseconds. The location of the virtual dipole moves with forward progress of the advancing wavefront. Unlike the situation in nerve tissue, the action potential duration in cardiac muscle ( $\sim 300$  msec) is long with respect to the time for complete depolarization of ventricular muscle ( $\sim 10$  msec). As a result the current flows into the actively depolarizing zone from one direction only, creating a single effective dipole rather than two dipoles racing away from each other in opposite directions.

It is easy to find the specific quantitative expression for the dipole moment product,  $kp$ , at the time of the R wave of the electrocardiogram for a transmural segment of area  $A$ . Using expression (13) for  $a$ ,  $\dot{V}_{\text{max}}$  for  $\dot{V}_1$ , and zero for  $\dot{V}_2$  we have for the R wave

$$kp_R = \frac{1}{2\pi} \cdot \frac{\rho A V_m^2 C_m \sigma_{\text{icf}} v^2}{\dot{V}_{\text{max}} r_c} \quad (14a)$$

Similarly, we can modify the general expression (11) for the whole heart to obtain the body surface potential created by a normal whole heart at the time of the R wave as

$$V(P) = \frac{\rho C_m V_m^2 \sigma_{\text{icf}} v^2}{2\pi r_c \dot{V}_{\text{max}}} \cdot \sum_n A_n \cdot \frac{\cos(\theta_n)}{r_n^2} \quad (14b)$$

This equation 14(b) will be used in the Results section to create a quantitative prediction of body surface potentials in three dimensions at the time of the R wave. It is also possible to predict quantitatively the amplitudes of other electrocardiographic waves.

### Electrical recovery—the T wave

After the wave of excitation has traversed all ventricular muscle, the flat ST segment of the electrocardiogram appears during mid ventricular systole. Toward the end of systole repolarization begins, as charges are pumped onto membrane capacitances of individual myocytes during the falling phase of the transmembrane action potential. The nature of this electrical recovery is rather different from that of electrical excitation. Compared to the short time of depolarization, about 0.5 msec, repolarization in cardiac muscle takes about 100 msec. There is no wavefront speeding through space, in which one cell triggers another like a chain of dominoes. Instead all of the cells return to resting membrane potential gradually, but with some areas leading and others lagging in time. Further, membrane recharging is an energy-dependent process and is governed by local metabolism and temperature. Areas with relatively poor blood supply, such as the subendocardium or areas affected by coronary artery disease, tend to repolarize more slowly<sup>15</sup>.

In terms of the equivalent dipole concept, the situation during the T wave of the electrocardiogram can be regarded as shown in Fig. 4. A column of myocardium of cross sectional area  $A$  is divided into two equal length zones of differing metabolic rate. Zone 2 recovers faster than zone 1, and so the local outward transmembrane currents  $i_1$  and  $i_2$  differ, with  $i_2 > i_1$ . Let  $\bar{i}$  represent the average repolarization current for the whole column. We can represent the ion pumping of the two zones in terms of a small fractional difference,  $\varepsilon$ , such that

$$i_1 = \bar{i} \left( 1 - \frac{\varepsilon}{2} \right) \quad \text{and} \quad i_2 = \bar{i} \left( 1 + \frac{\varepsilon}{2} \right). \quad (15)$$

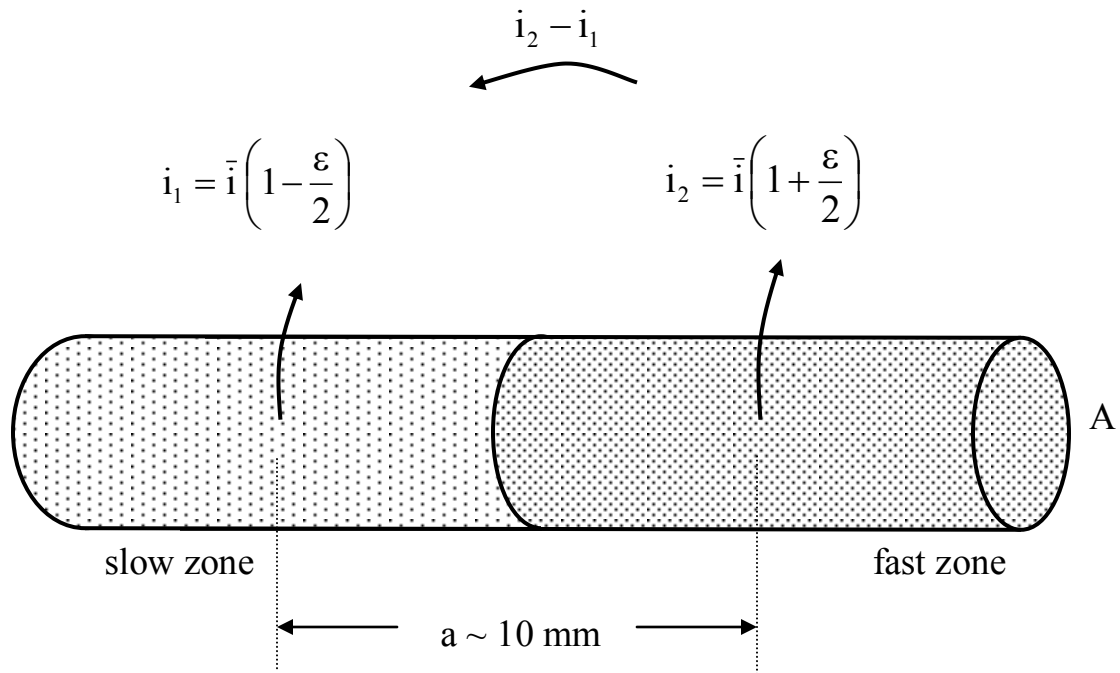


**Fig. 4.** Current flows responsible for creation of an effective dipole between zones of faster recovering and slower recovering tissue during the T wave of the electrocardiogram. The variable  $\varepsilon$  is the fractional difference in rates of repolarization. Here the effective length,  $a$ , is much larger than for depolarization in Fig. 3.

For example, if zone 2 repolarizes at 110% of the average rate and zone 1 repolarizes at 90% of the average rate, then  $\varepsilon = 20\%$ . As the membranes are repolarizing, the difference in recharge current, namely  $i_2 - i_1 = \bar{i} \varepsilon$ , will flow from zone 2 to zone 1, creating a virtual dipole with its axis parallel to the axis of the column. The ion pumps in the stronger zone will help out their weaker neighbors so that the total charge for the column comes back to the resting level at the end of the T wave, with the more metabolically able myocytes doing more work.

To predict the relative amplitude of the T wave compared to that of the QRS complex it is sufficient to compare the dipole moment product per unit of cross sectional area for repolarization  $(kp/A)_T$  versus that for depolarization  $(kp/A)_R$ . Note that the fractional difference in currents is equal to the fractional difference in transmembrane potential

slopes. That is  $\varepsilon = \frac{i_2 - i_1}{\bar{i}} = \frac{\dot{V}_1 - \dot{V}_2}{\dot{V}}$ . Hence the ratio of expression (10) for the T wave

to expression (10) for the R wave becomes

$$\frac{(kp/A)_T}{(kp/A)_R} = \frac{a_{\text{repol}}^2 \varepsilon \dot{V}_{\text{repol}}}{a_{\text{depol}}^2 \dot{V}_{\text{max}}} = \frac{a_{\text{repol}}^2 t_{\text{depol}}}{a_{\text{depol}}^2 t_{\text{repol}}} \cdot \varepsilon. \quad (16)$$

In (16) the ratio of slope  $\dot{V}_{\text{repol}}$  to slope  $\dot{V}_{\text{max}}$  is  $t_{\text{depol}}/t_{\text{repol}}$ , since repolarization must restore the original membrane charge. The duration of repolarization during Phase 4 of the action potential,  $t_{\text{repol}}$ , is much longer than the duration of depolarization in Phase 0,  $t_{\text{depol}}$ . Also the separation distances between tissues of different membrane charge is much greater in the case of repolarization. Hence the dipole moments for excitation and recovery are not dramatically different.

As an initial check on the validity of (16), suppose zone 1 represents subepicardial half of ventricular thickness in a human heart and zone 2 represents the subendocardial half. Then, assuming half the ventricular wall thickness is 7.5 mm, we have  $a_{\text{repol}}/a_{\text{depol}} \approx 7.5 \text{ mm} / 0.5 \text{ mm} = 15$  and  $t_{\text{depol}}/t_{\text{repol}} \approx 0.5 \text{ msec} / 100 \text{ msec} = 1/200$ . Hence from (16) we can predict that

$$\frac{(kp/A)_T}{(kp/A)_R} \approx \frac{225}{200} \cdot \varepsilon \approx \varepsilon.$$

If the difference in metabolic performance of zones 1 and 2 is 25%, the maximal T wave amplitude will be about 25% of the amplitude of the R-wave, roughly as is observed. The actual amplitude of the repolarization wave will be determined by local metabolic factors and local geometry in health and disease and will be more variable than the amplitude of the R-wave, as is observed. However, we can expect that T waves will be roughly a quarter as tall as R waves in typical cases. The net dipole vector for cardiac repolarization from all muscle columns in the heart, if constructed from an origin near the

center of the heart, will point away from slowly repolarizing regions toward faster repolarizing ones. If the local recovery rates are equal, then the T wave dipole will be zero.\*

### Electrical injury—ST segment shifts

The so-called "current of injury"<sup>1, 16</sup> flowing between acutely injured myocardium and nearby normal myocardium has multiple causes as a result of complex underlying pathophysiology during the first few minutes of ischemia<sup>17, 18</sup>, including intracellular to extracellular leakage of potassium ions during anoxia<sup>17-19</sup> causing a greater local extracellular potassium ion concentration and unbalancing of the normal Nernst equilibrium<sup>14</sup> with reduction of resting transmembrane potential and consequent inactivation of fast sodium channels<sup>7, 8</sup>. Although electrophysiological mechanisms of acute injury remain a subject of active research, the essential phenomena for present purposes have been consistently demonstrated in microelectrode studies of injured cardiac myocytes. These are reduction in action potential amplitude and shortening of action potential duration in injured tissue, as shown in the classical microelectrode studies of Downar, Janse, and Durrer<sup>20</sup>. Electrophysiologic studies of cardiac muscle cells subjected to anoxia consistently demonstrate reduction in action potential duration<sup>10;</sup>

As sketched in Fig. 5(a), the slope of the action potential of injured tissue (dashed curve) during the time of the ST segment of the electrocardiogram is substantially steeper than the slope of the action potential of normal ventricular muscle during the time of the ST segment. This means that net outward transmembrane ionic currents in the injured and normal tissues differ. The difference leads to extracellular ionic current flow from the injured cardiac muscle into neighboring normal cardiac muscle during the ST segment. This extracellular current flow will create an effective local dipole, as indicated in Fig. 5(b). In particular, by the same reasoning as for expression (5)

$$i_2 - i_1 = \frac{2a_{ST}AC_m\sigma_{icf}}{r_c} \cdot (\dot{V}_1 - \dot{V}_2). \quad (17)$$

---

\* Interestingly, this analysis provides a nice explanation for the "hyperacute" ECG changes following experimental coronary artery occlusion. The very earliest ECG changes include high peaked T-waves for several minutes, which are followed soon after by the familiar ST-segment shifts. If the metabolic activity of subendocardial muscle in this setting falls to zero, but that in subepicardial muscle persists for a few minutes, then  $\varepsilon \approx 1$ , and we would expect T-waves about as tall as R waves, exactly as is observed in hyperacute stages of experimental myocardial infarction.

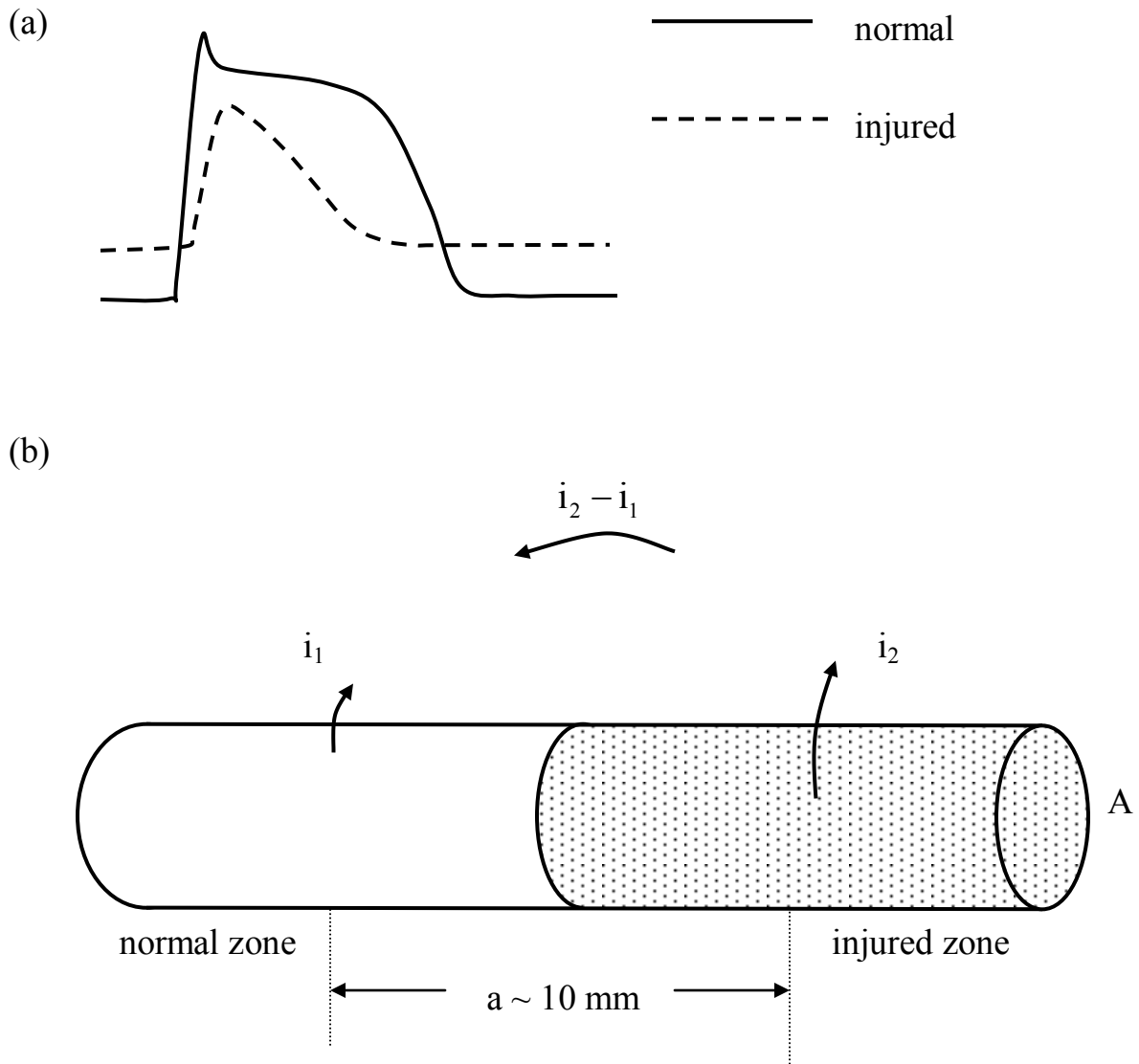


**Fig. 5.** Current flows responsible for creation of an effective dipole between zones of injured tissue and normal tissue during the ST segment of the electrocardiogram. The absolute value of the slope of the action potential is greater in injured tissue during this time interval than in normal tissue. As a result ionic current bleeds away from injured tissue.

If, as in the case of the normal T wave, we regard the difference in action potential slopes during the time of the ST segment as a fraction,  $\varepsilon'$ , of the normal repolarization slope during the T wave, then we can write as in expression (10)

$$kp_{ST} = \frac{1}{2\pi} \cdot \frac{\rho a_{ST}^2 AC_m \sigma_{icf}}{r_c} \cdot \dot{V}_{repol} \varepsilon', \quad (18)$$

and the relative strength of the ST segment dipole compared to that of the R wave dipole per unit of cross sectional area of myocardium is

$$\frac{(kp/A)_{ST}}{(kp/A)_R} = \frac{a_{ST}^2 \dot{V}_{repol} \varepsilon'}{a_{depol}^2 \dot{V}_{max}} = \frac{a_{ST}^2 t_{depol}}{a_{depol}^2 t_{repol}} \cdot \varepsilon'. \quad (19)$$

As an initial check on the validity of (19), assume a distance between source and sink of  $\sim 0.5$  mm for normal depolarization, as before, and  $\sim 7.5$  mm for injured tissue during the ST segment. Then we have  $a_{ST}/a_{depol} \approx 7.5 \text{ mm} / 0.5 \text{ mm} = 15$  and  $t_{depol}/t_{repol} \approx 0.5 \text{ msec} / 100 \text{ msec} = 1/200$ . Hence from (19) we would predict that

$$\frac{(kp/A)_{ST}}{(kp/A)_R} \approx \frac{225}{200} \cdot \varepsilon' \approx \varepsilon'.$$

For example, suppose that the slope of the action potential in injured tissue during the ST segment is 70 percent of the normal repolarization slope, as sketched in Fig. 5(a). Suppose that the slope of the action potential of normal tissue during the ST segment is only 10 percent of the normal repolarization slope, then we must have the slope difference during the ST segment,  $\varepsilon' = 70\% \text{ minus } 10\%$  or  $\varepsilon' = 0.6$ . The slope difference during the ST segment is 60% of the normal repolarization slope. In this case the magnitude of the ST segment shift would be nearly 60% of the height of the R wave. Such a prediction is consistent with ST segment shifts observed in experimental and clinical acute coronary occlusions.

## Results

### Quantitative prediction of R-wave amplitude

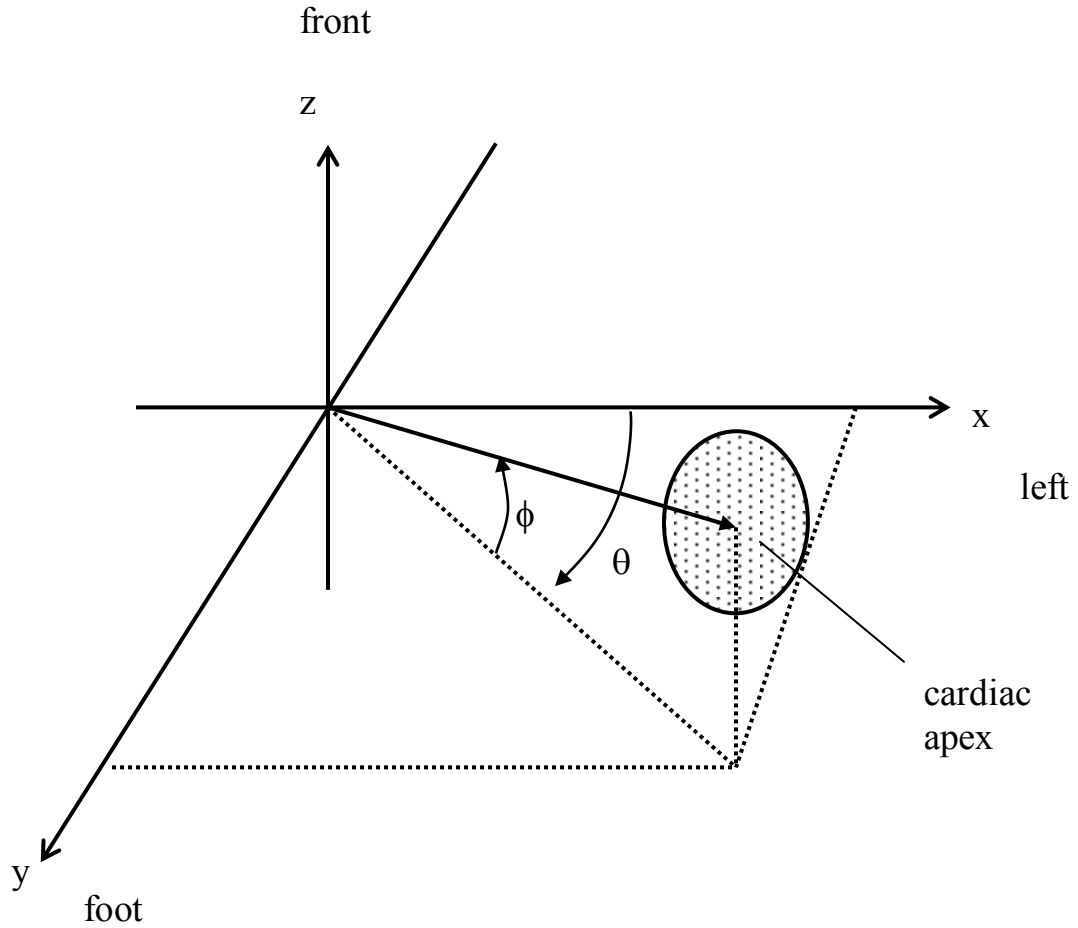
Values of the parameters in expressions(14a) and (14b) for a human adult are given in Table 1.

Table 1. Parameters for the quantitative dipole theory

Parameter	Value	Units	Reference
$\rho$	175	ohm-cm	Faes <sup>21</sup>
$V_m$	0.09	V	Boron <sup>14</sup> , Geddes <sup>1</sup>
$C_m$	1	$\mu\text{F}/\text{cm}^2$	Boron, Fozzard <sup>2,7</sup>
$\sigma_{icf}$	0.78		Friedman <sup>22</sup>
$\dot{V}_{\max}$	250	V/sec	Various <sup>3-5</sup>
$v$	100	cm/sec	Boron <sup>2,17</sup> , Myerberg <sup>23</sup>
$r_c$	$20 \times 10^{-4}$	cm	diFiore <sup>24</sup>
$kp_{\text{depol}}/\text{A}$	0.0035	Volts	

Using the values in Table 1 in Equation (14b), we may predict the amplitude of the R-wave and the entire map of body surface potentials. As a first approximation let us consider the apex of the left ventricle in isolation, which is aligned at approximately 45 degrees with respect to the head-to-foot axis, as indicated in Fig. 6, with  $\theta \approx 45$  degrees and  $\phi \approx 30$  degrees. Dipole vectors for radially oriented endocardial-to-epicardial muscle columns on opposite sides of the long axis of the ventricle point in opposite directions and largely cancel. Dipole vectors from muscle columns at the cardiac apex, however, are not opposed, owing to the presence of the 4 non-muscular cardiac valves at the base of the heart. Hence the apical ventricular muscle can be used as an initial approximation of the bioelectric source.

In Fig. 6 a disk-like cap of apical muscle is oriented at 45 degrees rotation from the horizontal plane toward the feet (inferiorly) and 30 degrees rotation toward the front (anteriorly). For human anatomy the radius of the apical disk is about 3 cm. Using expression (14) we can represent this disk approximately as a single dipole. The dipole moment for the lumped disk is (Table 1) is  $0.0035 \text{ Volts} * 28 \text{ cm}^2 = 0.1 \text{ Volt-cm}^2$ . At a distance of 10 cm the local surface potential in line with the axis of the apical dipole ( $\cos(\theta) = 1$ ) is  $kp/100 = 0.001 \text{ Volts}$ , or 1 millivolt. The corresponding off-axis potential on the other side of the heart would be perhaps  $-0.5$  millivolt, because of the tilt of the axis. So the roughly predicted R-wave amplitude in Lead II of the electrocardiogram (upper right chest to lower left chest) would be about 1.5 millivolts. This is a very reasonable estimate for R-wave amplitude obtained using a modified Lead II arrangement, as is done clinically, with a positive electrode on the upper left quadrant of the abdomen and a negative electrode on the right upper chest below the clavicle.



**Fig. 6.** Orientation of the cardiac apex in three dimensions within the chest in an initial model of cardiogenic body surface potentials. The origin of the coordinate system is in the center of the chest, as shown in Fig. 7. The angle of rotation ("longitude") is  $\theta$  the angle of elevation ("latitude") is  $\phi$ .

### Quantitative prediction of body surface potentials

To examine the predicted pattern of body surface potentials at the time of the R-wave using a laptop computer, one can place the single dipole, disk model in a chest-like generalized cylinder shown in Fig. 7. The cross section of the cylinder has half circle curves on each side and straight segments (sternum and back) in the middle that are equal in length to the radii of the half circles. Hence the profile has a single scale factor, the radius. Using a radius of 12 cm for an adult human model, the apical ventricular disk was placed at coordinates  $x_0, y_0, z_0$  (0 cm, 5 cm, 8 cm) and at angles of rotation and elevation of 45 degrees and 30 degrees, respectively. Then the potentials at surface points of the model were computed using (6b) and Microsoft Visual Basic code for this geometry with  $k_p = 0.1 \text{ Volt-cm}^2$ , as before.

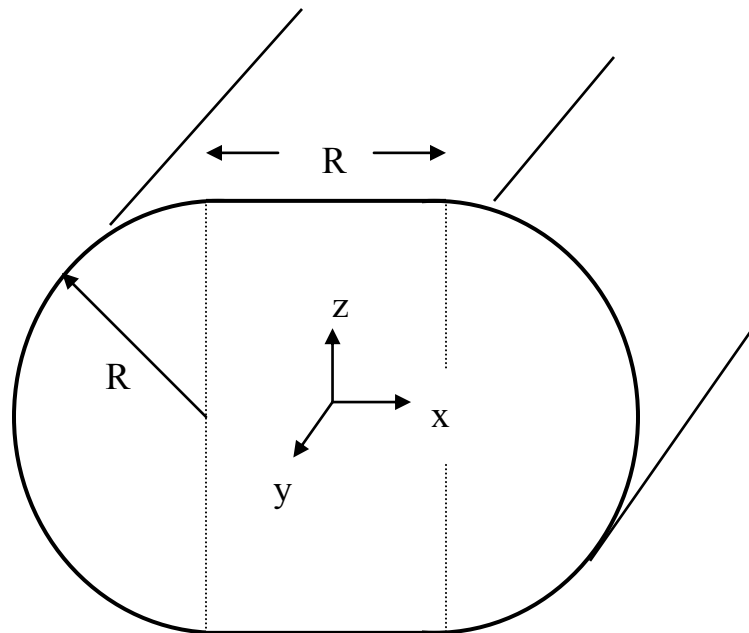


**Fig. 7.** Generalized cylindrical model of the chest for computation of body surface potentials. Anterior and posterior surfaces are straight segments. Sides of the rib cage are half circular curves.

The resulting body surface potential map is plotted in Fig. 8. The plane in Fig. 8 represents the chest wall, cut vertically at the right mid-axillary line and unwrapped. The left half of the map represents the front surface of the chest. The right half of the map represents the back surface of the chest. The vertical midline of the map is equivalent to the left mid-axillary line. The rectangular grid lines are 2 cm apart, and the curved isopotential contours represent 0.2 mV increments in voltage. Importantly, no arbitrary scale factors were used in calculations of body surface potentials. The roughly sinusoidal contour dividing potentials  $> 0$  and  $< 0$  indicates a plane of zero potential (so called "null plane")<sup>15</sup> passing through the chest cylinder in three dimensions. The null plane is orthogonal to the direction of the net cardiac dipole vector. Potentials on the back are largely negative. On the front there is a hot spot of positive potential near the cardiac apex. All of these features are similar to those observed in experimentally measured distributions of body surface potentials<sup>25-27</sup>. They are also similar to the calculated theoretical results of Miller and Geselowitz<sup>10</sup> (for example in their Figure 6), obtained using substantially more complex mathematics, and computed using an arbitrary scale factor to give a maximum potential of approximately 2 millivolts.

The next level of complexity for the bioelectric generator includes the lateral walls of the ventricles in addition to the cardiac apex. To investigate potentials from multiple dipoles around the entire curved surface of the ventricle at the time of the R-wave, the left ventricle was modeled as a three quarter spherical shell. The missing quarter sphere represents at the base of the heart and corresponds to the plane of the four heart valves, which are electrically inactive. The pole of the three quarter sphere opposite the base represents the cardiac apex, and a line from the center of the base to the apex represents the axis of the left ventricle. For simplicity, the entire three quarter sphere was assumed to have a continuous and simultaneous wavefront of depolarization propagating in the radial direction from endocardium to epicardium. The surface of the three quarter sphere was subdivided into 96 sectors, and the aggregate contribution of the 96 sector dipoles to surface potentials was calculated using expression (14b). This three quarter sphere represents a distributed multi-pole model of the heart.

To define a three quarter sphere numerically in a computer program a whole sphere was divided into sectors of latitude and longitude and only sectors a distance from the apex less than  $\sqrt{3}$  times the radius were included in the ventricular muscle model. This restriction omitted the area of the heart valves at the base of the heart as a source of electrical activity. For the multi-pole model, the origin of the three quarter sphere was placed at 3-dimensional coordinates  $x_0, y_0, z_0$  (3 cm, 0 cm, 3 cm), and the radius of the three quarter sphere was 4 cm. The apex was located at angles of rotation and elevation of 45 degrees and 30 degrees, respectively, with respect to the origin.

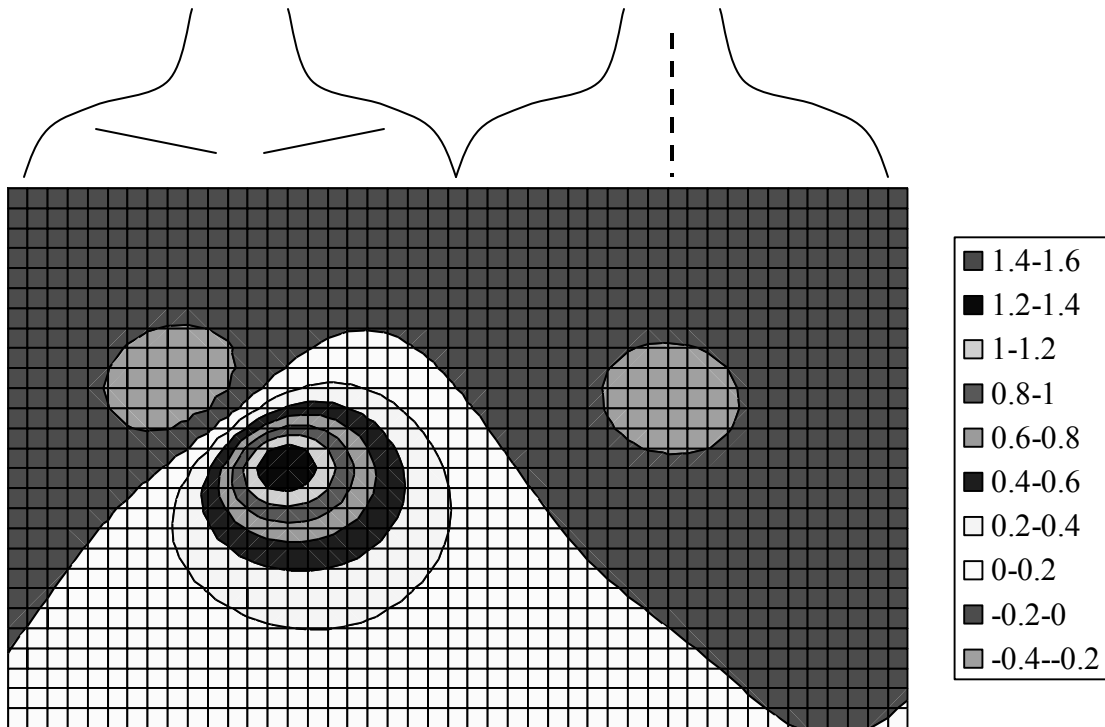


**Fig. 8.** Calculated body surface potentials for the initial model of Figs 6 and 7 including only an apical disk of ventricular tissue at the time of the R-wave of the electrocardiogram. The apical disk was centered at  $x_0, y_0, z_0 = 5 \text{ cm}, 0 \text{ cm}, 5 \text{ cm}$  and was oriented at  $\theta = 45$  degrees,  $\phi = 30$  degrees. The horizontal axis represents the full circumference of the chest with right and left edges joined at the right mid axillary line. Numerical values (legend) are in millivolts.

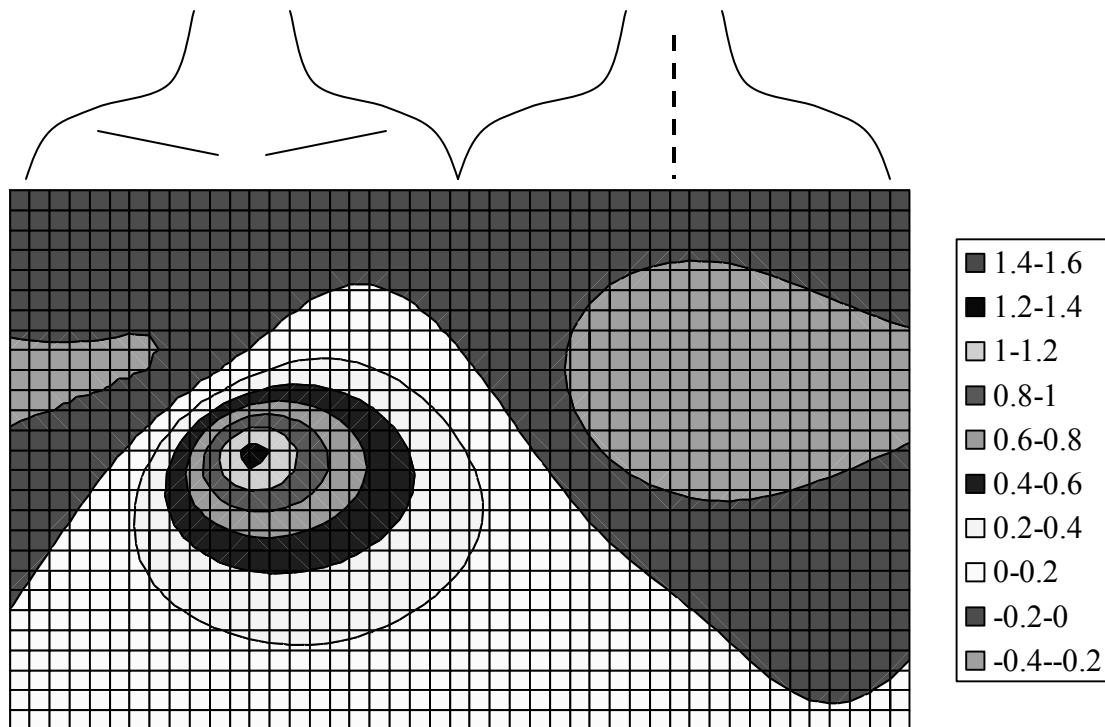


**Fig. 9.** Calculated body surface potentials at the time of the R-wave of the electrocardiogram for a distributed three-quarter sphere model of ventricular muscle having radius of 4 cm, center at  $x_0, y_0, z_0 = 3 \text{ cm}, 0 \text{ cm}, 3 \text{ cm}$  within the chest model of Fig. 7, and oriented at angles  $\theta = 45$  degrees and  $\phi = 30$  degrees, as defined in Fig. 6. The horizontal axis represents the full circumference of the chest with right and left edges joined at the right mid axillary line. Numerical values (legend) are in millivolts.

The resulting body surface potential map at the time of the R-wave is plotted in Fig. 9. The pattern of body surface potentials is similar to that in Fig. 8, with a somewhat greater lateral spreading of potentials associated with the more widely distributed sources. These quantitative calculations of chest surface potentials at the peak of the R-wave for a hypothetical human adult with parameters in Table 1 demonstrate quite realistic patterns and magnitudes of body surface potentials<sup>26-28</sup>. Despite the simplifying geometric assumptions, the isopotential contours show life-like complexity.

#### R-wave amplitudes in classical electrocardiographic leads

The R-wave amplitude for any particular lead configuration is implied by the body surface potential maps. For example, using a modified Lead II, as previously described, with positive and negative electrodes at the lower left and upper right borders of the anterior chest of an adult human (as is done in critical care units in hospitals), the measured potential difference in Fig. 9 would be approximately 0.7 – (-0.3) mV or 1.0 mV. The measured potential difference in Lead I (upper left chest vs. upper right chest) would be perhaps 0.2 – (-0.3) mV or 0.5 mV, etc. If the Wilson central terminal is taken as having zero potential, which is reasonable for this model, the R-wave amplitude for a chest lead such as V<sub>4</sub> would have an amplitude of about 1.2 mV. These values, obtained with no free parameters, are the proper order of magnitude for signals in the classical ECG leads.

#### Quantitative prediction of the P-wave

As atrial depolarization spreads from the SA node toward the AV node diagonally across the surface of the atria, roughly parallel to the axis of Lead II, the total cross section of active atrial muscle is perhaps 0.3 cm x 25 cm = 8 cm<sup>2</sup>, or about a quarter of the area of the apical ventricular disk. Hence the P-wave amplitude is about one fourth that of the R-wave. The beginning and end of the P-wave are gently tapered and continuous because initial and final depolarization tends to proceed more orthogonally to the Lead II axis.

#### Quantitative prediction of the T wave amplitude and ST-segment shifts with injury

As indicated by expressions (16) and (19) the amplitudes of T waves and ST segment shifts can be reckoned in terms of the fraction of normal repolarization current,  $\epsilon$  or  $\epsilon'$ , that flows between zones of rapidly versus slowly repolarizing tissue in the case of the T wave, or between zones of injured versus healthy tissue in the case of ST segment shifts. Approximate maximal amplitudes for the T wave and for ST segment shifts with injury are in the neighborhood of one third of the amplitude of the R wave for T waves and two thirds of the amplitude of the R wave for ST segment shifts, as are commonly observed in clinical electrocardiograms.

## Discussion

The elementary mathematical treatment herein described predicts the essential features and the magnitudes of the body surface potential field produced by cardiac activation and recovery. Such predictive dipole models provide a conceptually satisfying, physical explanation for the genesis of the P, QRS, and T waves of the normal electrocardiogram and the ST segment shifts of myocardial injury. This explanation is consistent with known physics, membrane physiology, histology, gross anatomy, and mathematics.

The forgoing analysis also predicts the classical electrocardiographic abnormalities of infarction and ischemia. Old, stable infarction is characterized by electrically inactive scar tissue that has replaced normal, active muscle. Clearly, component dipoles of excitation during the QRS complex of the electrocardiogram must drop out in areas of infarcted tissue. If the aggregate dipole of excitation is constructed from a point of origin near the center of the heart, the unbalancing of components causes a vector shift away from the infarct.

Ischemia without infarction is characterized by delayed repolarization of the ischemic area. In this case the component repolarization (T wave) dipoles will tend to point away from metabolically depressed tissue, toward metabolically vigorous tissue. Abnormally inverted T waves in certain leads facing the ischemic zone may result. In the case of acute injury, ST segment dipoles will point from normally depolarized myocardium toward areas of partially polarized, injured tissue, often pinpointing the sector of ventricular wall that is injured. Each of these predictions is consistent with routine clinical observations<sup>15</sup>.

This simplified, predictive dipole theory can be taught to students of physiology who understand the concepts of transmembrane action potentials and impulse conduction velocity in the heart, together with some basic gross anatomy, histology, and mathematics. It predicts how many millivolts of potential difference on the body surface are expected on the basis of textbook anatomy and physiology, without the use of arbitrary scale factors. Streamlined understanding of the cardiac bioelectric generator along these lines may lead to more confident and sophisticated vector interpretation of ECGs in the future and can today provide a meaningful answer for thinkers who have wondered how body surface potentials are linked quantitatively to transmembrane action potentials and currents in cardiac muscle cells.

## References

1. Geddes LA, Baker LE. Principles of Applied Biomedical Instrumentation, Second edition. John Wiley & Sons, New York, 1975.
2. Lines GT, Buist ML, Grottum P, Pullan AJ, Sundnes J, Tveito A. Mathematical models and numerical methods for the forward problem in cardiac electrophysiology. *Computing and Visualization in Science* 2003; 5:215-239.
3. Clark J, Plonsey R. The extracellular potential field of the single active nerve fiber in a volume conductor. *Biophys J* 1968; 8:842-64.
4. Geselowitz DB. On the theory of the electrocardiogram. *Proceedings of the IEEE* 1989; 77:857-876.
5. Rudy Y, Plonsey R. A comparison of volume conductor and source geometry effects on body surface and epicardial potentials. *Circ Res* 1980; 46:283-91.
6. Gulrajani RM. The forward problem of electrocardiography: from heart models to body surface potentials. *Proceedings 19th International Conference IEEE/EMBS* 1997:2604-2609.
7. Selvester RH, Solomon JC, Gillespie TL. Digital computer model of a total body ECG surface map: adult male torso simulation with lungs. *UCLA Forum Med Sci* 1970; 10:369-76.
8. Barr RC, Pilkington TC, Boineau JP, Spach MS. Determining Surface Potentials from Current Dipoles, with Application to Electrocardiography. *IEEE Transactions on Bio-medical Engineering* 1966; BME-13:88-92.
9. Gelernter HL, Swihart JC. A Mathematical-Physical Model of the Genesis of the Electrocardiogram. *Biophys J* 1964; 4:285-301.
10. Miller WT, Geselowitz DB. Simulation studies of the electrocardiogram. I. The normal heart. *Circ Res* 1978; 43:301-15.
11. Gentet LJ, Stuart GJ, Clements JD. Direct measurement of specific membrane capacitance in neurons. *Biophys J* 2000; 79:314-20.
12. Kip AF. *Fundamentals of Electricity and Magnetism*. New York: McGraw-Hill, 1969:630.
13. Selby SM. *CRC Standard Mathematical Tables*. Cleveland, 1975:756.
14. Boron WF, Boulpaep EL. *Medical Physiology*. Philadelphia: Elsevier, 2005:1319.
15. Grant RP. R.P. Grant, *Clinical Electrocardiography: The Spatial Vector Approach*. New York: McGraw-Hill, 1957.
16. Hoff HE, Nahum LH. The electrocardiographic localization of myocardial infarcts by injury currents and ventricular extrasystoles. *Am J Physiol* 1945; 143:723-720.
17. Wilde AA, Escande D, Schumacher CA, et al. Potassium accumulation in the globally ischemic mammalian heart. A role for the ATP-sensitive potassium channel. *Circ Res* 1990; 67:835-43.
18. Shigematsu S, Arita M. Anoxia-induced activation of ATP-sensitive K<sup>+</sup> channels in guinea pig ventricular cells and its modulation by glycolysis. *Cardiovasc Res* 1997; 35:273-82.

19. Yan GX, Yamada KA, Kleber AG, McHowat J, Corr PB. Dissociation between cellular K<sup>+</sup> loss, reduction in repolarization time, and tissue ATP levels during myocardial hypoxia and ischemia. *Circ Res* 1993; 72:560-70.
20. Downar E, Janse MJ, Durrer D. The effect of acute coronary artery occlusion on subepicardial transmembrane potentials in the intact porcine heart. *Circulation* 1977; 56:217-24.
21. Faes TJ, van der Meij HA, de Munck JC, Heethaar RM. The electric resistivity of human tissues (100 Hz-10 MHz): a meta-analysis of review studies. *Physiol Meas* 1999; 20:R1-10.
22. Friedman SM, Friedman CL, Nakashima M. Sodium gradient and renoprival hypertension in the rat. *Circ Res* 1959; 7:917-25.
23. Myerburg RJ, Gelband H, Nilsson K, Castellanos A, Morales AR, Bassett AL. The role of canine superficial ventricular muscle fibers in endocardial impulse distribution. *Circ Res* 1978; 42:27-35.
24. diFiori MSH. *Atlas of Human Histology*. Philadelphia: Lea & Febiger, 1981:267.
25. Taccardi B. Distribution of heart potentials on the thoracic surface of normal human subjects. *Circ Res* 1963; 12:341-52.
26. Klug D, Ferracci A, Molin F, et al. Body surface potential distributions during idiopathic ventricular tachycardia. *Circulation* 1995; 91:2002-9.
27. Hanninen H, Takala P, Rantonen J, et al. ST-T integral and T-wave amplitude in detection of exercise-induced myocardial ischemia evaluated with body surface potential mapping. *J Electrocardiol* 2003; 36:89-98.
28. De Ambroggi L, Bertoni T, Locati E, Stramba-Badiale M, Schwartz PJ. Mapping of body surface potentials in patients with the idiopathic long QT syndrome. *Circulation* 1986; 74:1334-45.

### Appendix 1: membrane surface area in a volume of heart muscle

Consider the aggregate surface area of cylindrical heart muscle cells with radius,  $r_c$ , that comprise volume fraction,  $\sigma_{icf}$ , of heart muscle tissue (the subscript "icf" indicating intracellular fluid). The total intracellular fluid in a volume  $V$  of muscle tissue is  $\sigma_{icf} V$ . The aggregate length of all such cells is the total cell volume divided by cell cross section or  $L = \frac{\sigma_{icf} V}{\pi r_c^2}$ . The aggregate membrane area is  $A_c = 2\pi r_c L = 2\pi r_c \cdot \frac{\sigma_{icf} V}{\pi r_c^2} = \frac{2\sigma_{icf} V}{r_c}$ . In

turn, the total membrane area per unit volume of tissue is  $\frac{A_c}{V} = \frac{2\sigma_{icf}}{r_c}$ .

### Appendix 2: the near field around a dipole and its midline slope

Consider a dipole comprised of opposite charge clusters  $-q$  and  $+q$  separated by distance,  $a$ , as shown in Fig. A2.1

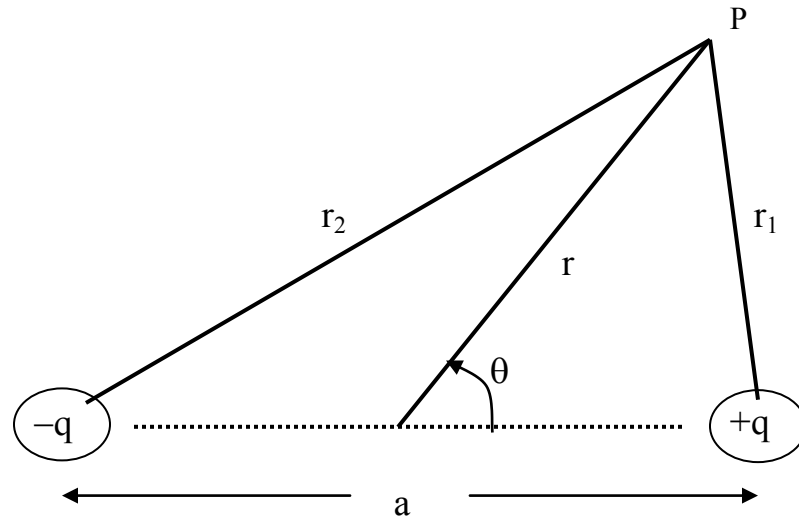


**Fig. A2.1.** Definitions of a classical dipole.

We seek the combined potential,  $V_P$ , at arbitrary field point,  $P$ , located at distances  $r_1$  from  $+q$ ,  $r_2$  from  $-q$ , and  $r$  from their midpoint. Vector  $r$  makes angle  $\theta$  with respect to the axis of the dipole, as shown.  $V_P$  is a function of  $r$  and  $\theta$  only because of cylindrical symmetry. The distances are related by the Law of Cosines as follows

$$r_1^2 = r^2 + \left(\frac{a}{2}\right)^2 - ra \cos(\theta)$$

$$r_2^2 = r^2 + \left(\frac{a}{2}\right)^2 - ra \cos(\pi - \theta) = r^2 + \left(\frac{a}{2}\right)^2 + ra \cos(\pi)$$

Adding the electrical potentials,  $V = kq/r$ , for the two point charges we have,

$$V_p = kq \left\{ \frac{1}{r_1} - \frac{1}{r_2} \right\} = kq \left\{ \frac{1}{\sqrt{r^2 + a^2/4 - ra \cdot \cos(\theta)}} - \frac{1}{\sqrt{r^2 + a^2/4 + ra \cdot \cos(\theta)}} \right\},$$

which is the net potential for a general dipole. In addition, we are especially interested in the slope of the dipole's potential field across the midline, which by differentiation in polar coordinates is

$$\frac{dV_p}{d\theta} = -\frac{1}{2} kq \left\{ \frac{ra \cdot \sin(\theta)}{\left(r^2 + a^2/4 - ra \cdot \cos(\theta)\right)^{3/2}} - \frac{-ra \cdot \sin(\theta)}{\left(r^2 + a^2/4 + ra \cdot \cos(\theta)\right)^{3/2}} \right\}.$$

For midline point  $(r, \theta)$  we have  $\theta = 90$  degrees,  $\sin(\theta) = 1$  and  $\cos(\theta) = 0$ , so that

$$\frac{dV_p(90^\circ)}{d\theta} = -kq \left\{ \frac{ra}{\left(r^2 + a^2/4\right)^{3/2}} \right\} = -\frac{kpr}{\left(r^2 + a^2/4\right)^{3/2}},$$

where the dipole moment is  $p = kq$ . The negative sign indicates that as  $\theta$  increases, the potential decreases.

Appendix 3: nomenclature

<b>Symbol</b>	<b>Definition</b>	<b>Units</b>
A	area	cm <sup>2</sup>
a	distance between charges in a diopole	cm
C	total membrane capacitance in a tissue volume	μF
C <sub>m</sub>	specific membrane capacitance per unit area	μF/cm <sup>2</sup>
ε, ε'	fractions of normal repolarization current flowing from one region to another	
i	current	amperes
k	permittivity constant -- 1/(4πε <sub>0</sub> K)	V-cm / coulomb
kp/A	normalized dipole moment	Volts
p	dipole moment	coulomb-cm
ρ	tissue resistivity	ohm-cm
π	circle ratio, 3.14159. . .	
Q	charge on membrane capacitance	coulombs
q	point charge	coulombs
R	radius of curvature of chest wall model	cm
r	distance from bioelectric source to field point on body surface	cm
r <sub>c</sub>	radius of a cylindrical cardiac muscle cell	cm
σ <sub>icf</sub>	volume fraction of cells in tissue (intracellular fluid fraction)	
t	time	sec
θ, φ	angles	degrees or radians
V	instantaneous transmembrane potential	V/sec
V <sub>m</sub>	transmembrane resting potential	Volts
$\dot{V}$	time rate of change of the transmembrane action potential	Volts/sec
$\dot{V}_{\max}$	rate of rise of the action potential during Phase 0	Volts/sec
V <sub>P</sub>	body surface potential at point, P	Volts or millivolts
v	impulse conduction velocity	cm/sec
x, y, z	spatial coordinates in three dimensions	cm